Carbon 129 (2018) 374–379

Contents lists available at ScienceDirect

Carbon

journal homepage: www.elsevier.com/locate/carbon

Highly efficient water desalination in carbon nanocones

Wen Li [a, b, 1], Wensen Wang [a, 1], Yingnan Zhang [a], Youguo Yan [a], Petr Král [b, c, d, *], Jun Zhang [a, **]

[a] College of Science, China University of Petroleum (East China), Qingdao, Shandong 266580, People's Republic of China
[b] Department of Chemistry, University of Illinois at Chicago, Chicago, IL 60607, United States
[c] Department of Physics, University of Illinois at Chicago, Chicago, IL 60607, United States
[d] Department of Biopharmaceutical Sciences, University of Illinois at Chicago, Chicago, IL 60607, United States

ARTICLE INFO

Article history:
Received 14 September 2017
Received in revised form
21 November 2017
Accepted 9 December 2017
Available online 12 December 2017

ABSTRACT

Inspired by the highly efficient water transport presented in hourglass-shaped aquaporin channels, molecular dynamics simulations were conducted to study water desalination in carbon nanocones (CNCs). Their desalination performance (salt rejection, water flow) depends on the cone size, angle, and flow direction (nonequilibrium). Free energy calculations reveal that ultrasmall CNCs with apex angles of 19.2° provide the best desalination performance, since they contain relatively ordered water structures, providing high water flows, but have a high ion rejection rate. The desalination performance observed in these CNCs is better than in nanoporous graphene and MoS_2 monolayers.

1. Introduction

Freshwater shortage is becoming a worldwide problem due to a global climate change, growing population, and increasing industrial and agricultural consumptions [1,2]. Seawater covers 70% of earth surface [3] and could provide a plentiful resource of freshwater, if efficient desalination methods are developed. However, due to a large energy consumption and trade-off between water permeability and salt rejection rate [4], the desalination efficiency is unsatisfactory in currently used reverse osmosis (RO) methods [5].

In carbon nanotubes (CNT) [6,7], water can flow almost without friction, since its flow rate is 4–5 orders of magnitude larger than predicted by a classical fluid-flow theory [8]. Efficient desalination membranes have been constructed using aligned ultranarrow CNTs [9–11]. Efforts were also made to prepare highly permeable and selective ultrathin membranes based on nanoporous graphene [12–19], graphyne [20,21], molybdenum disulfide (MoS_2) [22,23], and other 2D materials [24–26]. Many of these nanoporous materials have a large potential in water desalination, since they have a high water permeability and salt rejection rates.

Nature provides great inspiration by its design principles and solutions. For example, biological channels in cell membranes are highly selective, permeable, and environmentally sensitive [27–30], which is difficult to achieve simultaneously in synthetic nanochannels [31–35]. Due to a high water permeability and selectivity, aquaporins (AQPs) play a crucial role in the passage of water across cell membranes [36]. AQPs have an hourglass-shaped channel structure [37,38], in which the narrow neck is responsible for a high water selectivity, and the conical entrance for a high water permeability (reduced hydrodynamic entrance resistance). In principle, similar conical structures could enhance fluidic flow in synthetic nanochannels [38–43]. Inspired by the nearly frictionless water flow in CNTs and the highly permeable and selective water flow in conical AQPs, we assume that a high desalination performance can be achieved in carbon nanocones (CNCs). Here, we perform molecular dynamics (MD) simulations to examine this possibility.

2. Models

Fig. 1 shows the studied model system. A fixed CNC of a 2 nm length is held between two fixed graphene sheets with pores matching the CNC channel. Two more (rigid) graphene slabs were used to maintain constant pressures at the left and right regions of the system. When the desalination took part from the base (tip) to the tip (base) sides, salt water (0.5 mol/L NaCl) was left at the left (right) of the CNC channel (high pressure region), and pure water

* Corresponding author. Department of Chemistry, University of Illinois at Chicago, Chicago, IL 60607, United States.
** Corresponding author. College of Science, China University of Petroleum (East China), Qingdao, Shandong 266580, People's Republic of China.
E-mail addresses: pkral@uic.edu (P. Král), zhangjun.upc@gmail.com (J. Zhang).
[1] Wen Li and Wensen Wang contributed equally.

https://doi.org/10.1016/j.carbon.2017.12.039
0008-6223/

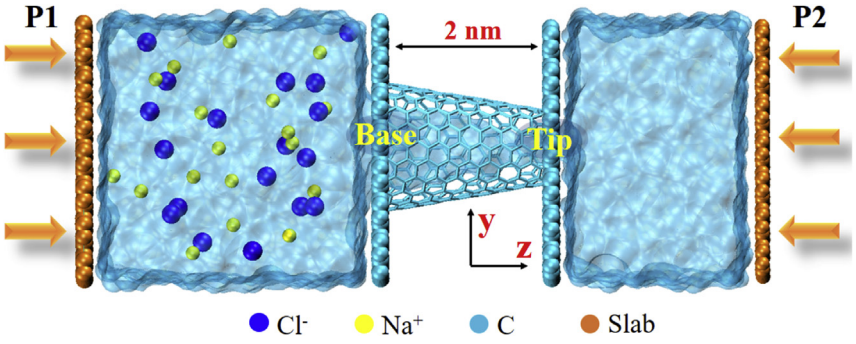

Fig. 1. The constructed system used in this work. Water was shown as transparent cyan. (A colour version of this figure can be viewed online.)

was put at the right (left) of the CNC channel (low pressure region -0.1 MPa). Periodic boundary conditions were applied in the X and Y directions.

The atomistic MD simulations were performed using LAMMPS [44] and a modified CHARMM force field. Water was described by a TIP3P model [45], where the SHAKE algorithm was used to keep the rigidity of water molecules. The ion-ion Lennard-Jones (LJ) parameters were obtained from literature [46], the carbon-carbon (sp^2 carbons) LJ parameters were $\sigma_{cc} = 0.33997$ nm and $\varepsilon_{cc} = 0.0859$ kcal/mol. Other LJ parameters were obtained using the Lorentz-Berthelot combining rules [47], as summarized in Table S1. The van der Waals (vdW) coupling was calculated with a cutoff of 12 Å and the particle-Particle-Particle-Mesh (PPPM) method was used for the calculation of long-range electrostatic interactions. The MD simulations were conducted in NVT ensemble at 298 K, with a time step of 1 fs, and the data were collected every 1 ps. The total simulation time of each system was 10 ns.

3. Results and discussion

Depending on the number of pentagons at the CNC apex [48], five symmetric CNCs exist with apex angles of 112.9°, 83.6°, 60.0°, 38.9° and 19.2°. Here, the CNCs tips were cut (Fig. 1) and their accessible pore areas are shown in Fig. S1 and described in Table S1. The tip pore areas in cut CNCs with apex angles of 19.2°, 38.9° and 60°, ranging from 19.30 to 19.37 $Å^2$, are similar to 19.29 $Å^2$ for (6, 6) CNT and 19.38 $Å^2$ for a nanoporous graphene (GN), which could both be used for desalination [49]. All the studied models are shown in Fig. S2.

First, we studied desalination under different hydrostatic pressures in a cut CNC with an apex angle of 19.2° (CNC-19.2°) and a tip pore area of 19.30 $Å^2$, as shown in Fig. S3. An approximately linear relationship between the pressure and water flux, but a full ion rejection, were observed. Therefore, in order to get enough statistics in a limited simulation time, a relatively large hydrostatic pressure of 100 MPa was adopted in the following simulations. Using these conditions, we examine the desalination performance (water flux and ion rejection) of systems shown in Fig. S2.

Water flux. Fig. S4 shows a time-dependent flow of filtered water at hydrostatic pressure of 100 MPa from the base (tip) to tip (base) sides for systems shown in Fig. S2. The calculated water fluxes (slopes of the curves in Fig. S4) are shown in Fig. 2, and the error bar was given based on three separated simulations. In the (6,6) CNT, a water flux of ~15 #/ns passes under 100 MPa pressure, in agreement with previous studies [49]. Three observations also could be done from these simulations: (1) the CNC systems have higher water flux than the CNT and GN systems, (2) the flow rate depends on the CNC orientation (higher water flux emerges from the base to tip side) and (3) the water flux increases with the decreasing CNC apex angles and reaches a maximum at 19.2°.

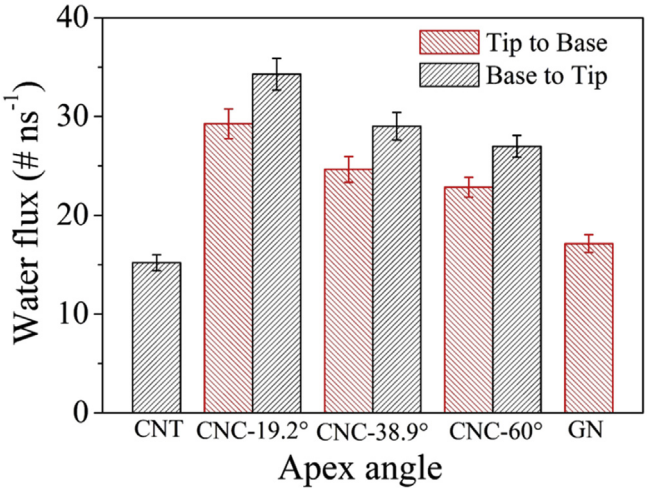

Fig. 2. Water flux from the base (tip) to tip (base) sides of CNCs with different apex angles. (A colour version of this figure can be viewed online.)

To understand the (1) point, the potential of mean forces (PMFs) of water was calculated in these channels to estimate the energy barriers for water transport (see SI for the detailed PMF calculation). Fig. 3a shows that in CNCs with larger angles the energy barrier decreases at the base side (cone diameter increases) but slightly increases at the tip side (cone diameter stays the same), where it eventually approaches the barrier presented in GN with the same diameter as the CNCs tips. This could explain why the smallest water flux is present in GN. Similarly, in the chosen CNT, the energy barrier is on average larger than in all the other systems, which gives the weakest water flux. To further understand the larger water flux in CNC channels quantitatively, we calculated the average axial velocity of water molecules passing through the CNT, GN and the tip side of the CNC channels (Table S2). We can see water molecules in CNC channels have larger velocities, which also indicate their larger water flux than that of CNT or GN systems.

When water flows in CNCs from the base to the tip sides, the gently increasing energy barriers permits a lot of water to enter, which contributes to their higher water flux. Similarly, when water flows in the opposite way, it can easily diffuse out of the channels, which also gives relatively larger flows. The larger base side pores in CNCs and the corresponding higher likelihood of collecting water from the solution under pressure (Fig. 3b) are responsible for higher water fluxes from the base to the tip sides, which explains the (2) point. However, this feature disappears at small pressures, since close to equilibrium both passage rates should be the same,

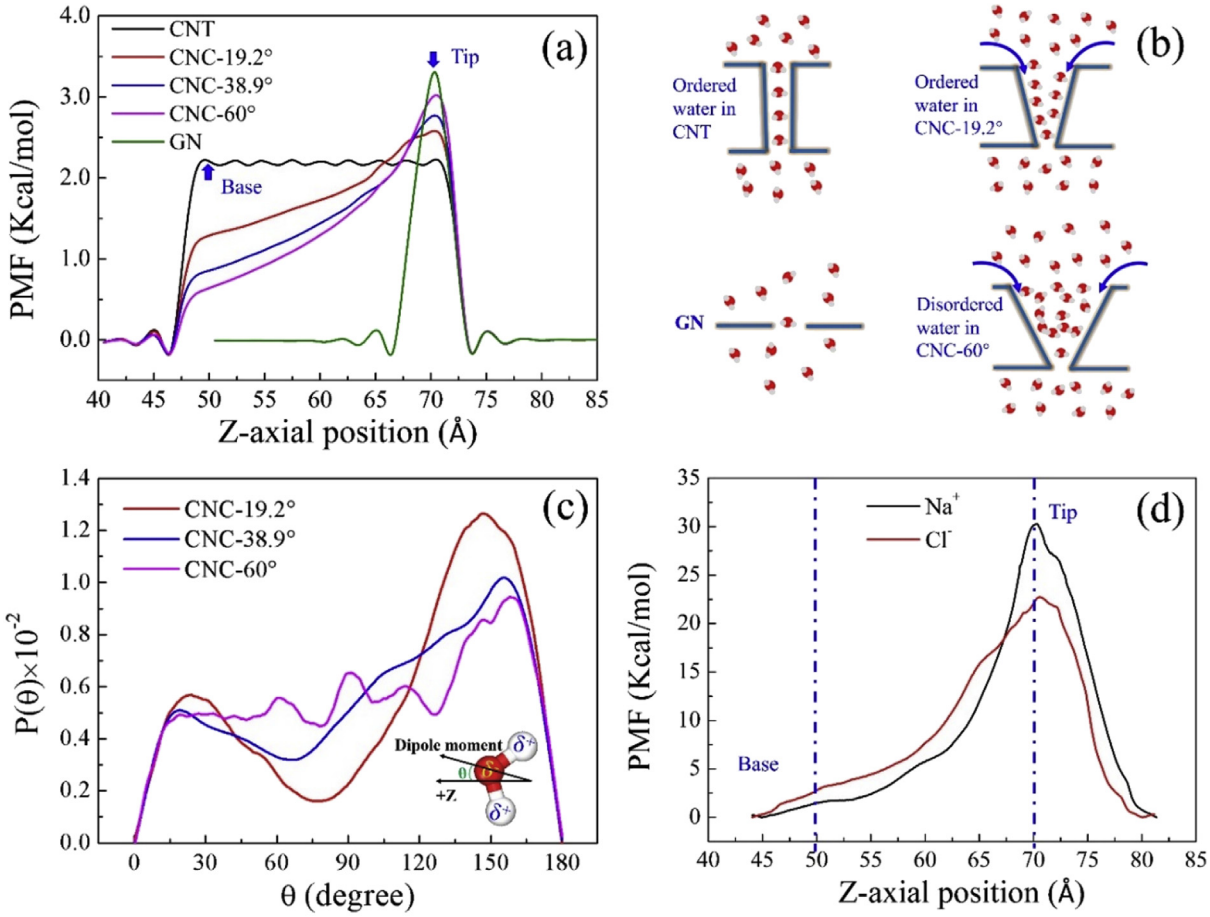

Fig. 3. (a) The potential of mean forces (PMFs) for water transport through the studied systems. (b) Cartoon representation of the water structure in the CNT, GN and CNCs with apex angles of 19.2° and 60°. (c) The probability distribution of water dipole orientation in CNC channels. (d) The PMFs for Na^+ and Cl^- passing through the CNC channel with apex angle of 19.2°. (A colour version of this figure can be viewed online.)

otherwise a spontaneous flow would be observed. There is still a higher flow in CNCs under such conditions, since either the molecules are better collected or better released than in the CNT or GN channels. Perhaps, systems that are conical both at their entrances and exits would have the largest flows.

To explain the (3) point, we can examine the nature of water flow inside CNCs by comparing it to the water flow in CNTs. In CNTs with nm-scale diameters, water becomes well arranged (like in crystals) and flows almost without friction [6,50], partly because the CNTs walls are non-polar and very flat (Fig. 3b) [51,52]. A small water permeability in CNTs is caused by their high entrance energy barriers (Fig. 3a). In nm-scale CNC-19.2°, water is still relatively ordered (Fig. 3b), but the average energy barrier is reduced compared to CNTs of the same entrance pore sizes (Fig. 3a). Consequently, water flows in such CNCs are larger. When the apex angle in CNCs is further increased, water molecules in the channels become less ordered, like in bulk water (CNC-60° system in Fig. 3b), which causes a reduction of their flow.

The ordering of water within these channels could be estimated from the probability distribution of water dipole orientation, P(θ) (Fig. 3c), where θ is an angle spanned by a water dipole vector and the Z-axis of the channel. In very thin CNTs, water is mostly oriented along the channel [53], which means that P(θ) has maxima around at 0° or 180°, while in CNC-19.2° the maxima are at 30° or 150°. A high probability around 90° indicates that water tends to flip and reorient frequently, the H-bond network also undergoes breaking and rebuilding, and water flows slower [53–55], as observed at CNCs with apex angles of 38.9° and 60° (Fig. 3c).

It should be noticed that in our simulations all the carbon atoms at the CNC channels are electroneutral. However, in a real system, the carbon atoms at the edge of the CNC channels are prone to be oxidized and develop small net charges. The net charges could polarize the passing water molecules and make the water molecules reorient themselves. Therefore, according to our above analysis, we think that the small net charges and the corresponding ordered water structure could further enhance the water flux [56,57].

Salt rejection. The percentage of ion rejection of the CNCs is calculated by the equation [58]: $R\ (\%)=(1-\ C_p/C_f) \times 100$, where C_p denotes the ratio of passed ion number with respect to passed water number, C_f denotes the initial salt concentration in feed box. From our results, all the systems in Fig. 2 could fully reject the passage of Na^+ and Cl^- ions with hydrated radius of 3.58 Å and 3.32 Å, respectively [59]. Since the smaller radius in all these pores is about the same, roughly 2.52 Å, the hydrated ions are rejected due to size exclusion. The ions should be dehydrated prior to passing through the channels, which is very difficult unless suitable charged groups and electronic polarization are considered to be present at the pore rim [12]. In Fig. 3d, the PMFs of Na^+ and Cl^- ions were also calculated to estimate the free energy barriers for ion transport in CNC-19.2° channel (see SI for the PMF calculation) [60,61]. Since ions would need to overcome a large energy barrier

(over than 20 kcal/mol), their entry in the channel is practically fully rejected. Moreover, the smaller Na^+ ion, with more strongly bound hydration waters, has a larger energy barrier. Note that our simulations are done in gradually changing conditions, since the ions concentration is increasing on the entry side. However, this effect has a negligible influence on the water flow over the simulation timescale (Fig. S4) [17,23,62].

CNCs with an optimal desalination performance. From these simulations, we can see that CNC-19.2° should have the best desalination performance. We can optimize the cone further by checking its tip within the range of 19.30 $Å^2$ to 50.64 $Å^2$ (Table S1 in SI), in order to gain a higher water flux, while keeping a desirable salt rejection rate. When the saline water goes through the channel from the base to tip (Fig. 4a), the water flux increases in larger tip pores, while the ion rejection rate decreases. When the flow is opposite, the water flux still increases, while the ion rejection rate is 100%, until the tip pore area reaches 50.64 $Å^2$. We can understand this as follows. For a flow from the base to tip side induced by pressure (Movie S1), multiple ions could enter the confined channel because of the large base side pore size. Then, the mutual pushing effects of the ions in the channel allows the first ion easier to dehydrate and pass through the channel (Fig. 4b–d), resulting in the low ion rejection rate. Meanwhile, the hydrated ions inside the channel could exert steric hindrance and slow down the water flow. This ion transport mode is similar to the Coulomb knock-on ion transport observed in biological ion channels [63], but here the driving force is external pressure. Therefore, this phenomenon could be called a pressure knock-on ion transport. This transport cannot work from the tip to base side (Movie S2), because of the absence of confined space to accommodate multiple ions. The entering ion could easily jump back to the solution once it encounters the energy barriers near the tip pore. Therefore, the blockage effect of the ion for water flow is negligible (Fig. S5). This also explains that why water flux from base to tip is higher than the flux from tip to base whereas it is opposite when pore area exceeds 35 $Å^2$ (see SI for detailed explanation). Consequently, a high ion rejection rate and high water flux could be achieved in a tip to base flow (Fig. 4). However, all these differences are only present due to relatively large pressures.

Supplementary data related to this article can be found at https://doi.org/10.1016/j.carbon.2017.12.039.

Comparison with other desalination membranes. CNC-19.2° with a tip pore area of 44.74 $Å^2$ gives the optimal desalination performance. Further comparison with commercial and other state-of-the-art atomic membranes was conducted and depicted in Fig. 5. It shows that the chosen CNC has exceptional high water

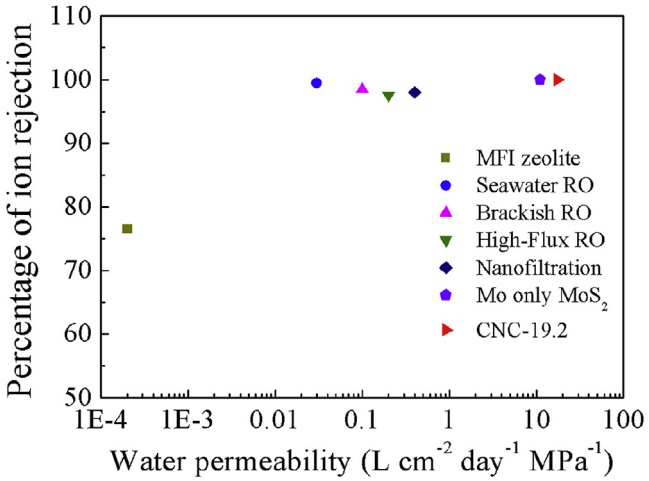

Fig. 5. The ion rejection and water permeation rate for various membranes (MFI-type zeolite [64], seawater RO [65], brackish RO [65], nanofiltration [65], high-flux RO [65], and Mo only MoS_2 [22]). (A colour version of this figure can be viewed online.)

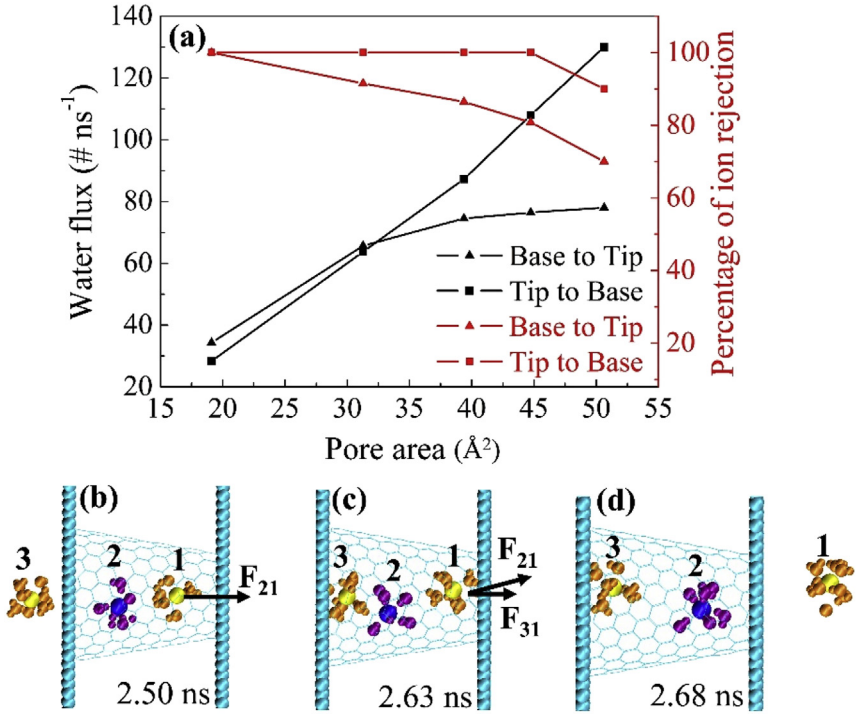

Fig. 4. (a) The water flux and percentage of ion rejection when ionic solution flows from the base (tip) to tip (base) of the 19.2° CNC channel under different accessible tip pore areas. (b–d) Pressure induced knock-on ion transport from the base to tip side. The orange and purple balls show the water molecules in the hydrated shell of Na^+ and Cl^-, respectively. (A colour version of this figure can be viewed online.)

permeability (17.43 L cm^{-2} day^{-1} MPa^{-1}), which is more than two orders of magnitude higher than in commercial RO membranes (0.03–0.4 L cm^{-2} day^{-1} MPa^{-1}). It is also ~60% higher than the recently developed ultrathin nanoporous MoS_2 membrane (10.97 L cm^{-2} day^{-1} MPa^{-1}) whose water permeability is ~70% higher than that of nanoporous graphene [22].

4. Conclusion

In this work, molecular dynamics simulations were conducted to investigate the desalination performance of CNCs. The results show that the CNCs could optimize water permeability compared with CNT and nanoporous graphene. In addition, CNC with apex angle of 19.2° provides largest water flow, due to a low entrance energy barrier and an ordered water structure present in the channel. Under pressure, CNCs also exhibit better desalination performance when the saline water goes from the tip to base side. Now, uniform CNC arrays have been synthetized by plasma-assisted self-organized growth [66] and through sharpening of CNC tips during plasma-assisted growth, including CNCs with different tip sizes [67]. Therefore, fabricating CNC membranes with uniform configuration and accurate pore sizes for desalination will come true in the near future. This work provides great promise for the next generation of desalination devices.

Acknowledgement

This work is financially supported by National Basic Research Program of China (2015CB250904), National Natural Science Foundation of China (51302321), Key Laboratory of Tectonics and Petroleum Resources (TPR-2016-16) and Fundamental Research Funds for the Central Universities (15CX08003A, 14CX0222A, 15CX05049A).

Appendix A. Supplementary data

Supplementary data related to this article can be found at https://doi.org/10.1016/j.carbon.2017.12.039.

Notes

The authors declare no competing financial interest.

References

[1] R.I. McDonald, P. Green, D. Balk, B.M. Fekete, C. Revenga, M. Todd, M. Montgomery, Urban growth, climate change, and freshwater availability, Proc. Natl. Acad. Sci. Unit. States. Am. 108 (15) (2011) 6312–6317.
[2] B.D. Negewo, Renewable Energy Desalination: An Emerging Solution to Close the Water Gap in the Middle East and North Africa, World Bank Publications, 2012.
[3] M. Chang, Forest hydrology: An Introduction to Water and Forests, CRC Press, 2006.
[4] H.B. Park, J. Kamcev, L.M. Robeson, M. Elimelech, B.D. Freeman, Maximizing the right stuff: the trade-off between membrane permeability and selectivity, Science 356 (6343) (2017) 1–10.
[5] A. Khalifa, H. Ahmad, M. Antar, T. Laoui, M. Khayet, Experimental and theoretical investigations on water desalination using direct contact membrane distillation, Desalination 404 (2017) 22–34.
[6] A. Kalra, S. Garde, G. Hummer, Osmotic water transport through carbon nanotube membranes, Proc. Natl. Acad. Sci. Unit. States. Am. 100 (18) (2003) 10175–10180.
[7] S. Joseph, N. Aluru, Why are carbon nanotubes fast transporters of water? Nano Lett. 8 (2) (2008) 452–458.
[8] M. Majumder, N. Chopra, R. Andrews, B.J. Hinds, Nanoscale hydrodynamics: enhanced flow in carbon nanotubes, Nature 438 (7064) (2005) 44.
[9] R. Das, M.E. Ali, S.B.A. Hamid, S. Ramakrishna, Z.Z. Chowdhury, Carbon nanotube membranes for water purification: a bright future in water desalination, Desalination 336 (2014) 97–109.
[10] H.Y. Yang, Z.J. Han, S.F. Yu, K.L. Pey, K. Ostrikov, R. Karnik, Carbon nanotube membranes with ultrahigh specific adsorption capacity for water desalination and purification, Nat. Commun. 4 (2013) 1–8.
[11] J. Yin, G. Zhu, B. Deng, Multi-walled carbon nanotubes (MWNTs)/polysulfone (PSU) mixed matrix hollow fiber membranes for enhanced water treatment, J. Membr. Sci. 437 (2013) 237–248.
[12] K. Sint, B. Wang, P. Král, Selective ion passage through functionalized graphene nanopores, J. Am. Chem. Soc. 130 (49) (2008) 16448–16449.
[13] K.A. Mahmoud, B. Mansoor, A. Mansour, M. Khraisheh, Functional graphene nanosheets: the next generation membranes for water desalination, Desalination 356 (2015) 208–225.
[14] D. Cohen-Tanugi, L.-C. Lin, J.C. Grossman, Multilayer nanoporous graphene membranes for water desalination, Nano Lett. 16 (2) (2016) 1027–1033.
[15] E.N. Wang, R. Karnik, Water desalination: graphene cleans up water, Nat. Nanotechnol. 7 (9) (2012) 552–554.
[16] D. Cohen-Tanugi, J.C. Grossman, Water permeability of nanoporous graphene at realistic pressures for reverse osmosis desalination, J. Chem. Phys. 141 (7) (2014), 074704.
[17] S.P. Surwade, S.N. Smirnov, I.V. Vlassiouk, R.R. Unocic, G.M. Veith, S. Dai, S.M. Mahurin, Water desalination using nanoporous single-layer graphene, Nat. Nanotechnol. 10 (5) (2015) 459–464.
[18] Y. Wang, Z. He, K.M. Gupta, Q. Shi, R. Lu, Molecular dynamics study on water desalination through functionalized nanoporous graphene, Carbon 116 (2017) 120–127.
[19] Y. Yan, W. Li, P. Král, Enantioselective molecular transport in multilayer graphene nanopores, Nano Lett. 17 (11) (2017) 6742–6746.
[20] J. Kou, X. Zhou, H. Lu, F. Wu, J. Fan, Graphyne as the membrane for water desalination, Nanoscale 6 (3) (2014) 1865–1870.
[21] M. Xue, H. Qiu, W. Guo, Exceptionally fast water desalination at complete salt rejection by pristine graphyne monolayers, Nanotechnol 24 (50) (2013), 505720.
[22] M. Heiranian, A.B. Farimani, N.R. Aluru, Water desalination with a single-layer MoS_2 nanopore, Nat. Commun. 6 (2015) 1–6.
[23] W. Li, Y. Yang, J.K. Weber, G. Zhang, R. Zhou, Tunable, strain-controlled nanoporous MoS_2 filter for water desalination, ACS Nano 10 (2) (2016) 1829–1835.
[24] K. Zhang, Z. He, K.M. Gupta, J. Jiang, Computational design of 2D functional covalent–organic framework membranes for water desalination, Environ. Sci. Water. Res. Technol. 3 (2017) 735–743.
[25] S. Dervin, D.D. Dionysiou, S.C. Pillai, 2D nanostructures for water purification: graphene and beyond, Nanoscale 8 (33) (2016) 15115–15131.
[26] H. Gao, Q. Shi, D. Rao, Y. Zhang, J. Su, Y. Liu, Y. Wang, K. Deng, R. Lu, Rational design and strain engineering of nanoporous boron nitride nanosheet membranes for water desalination, J. Phys. Chem. C 121 (40) (2017) 22105–22113.
[27] B. Corry, S.H. Chung, Mechanisms of valence selectivity in biological ion channels, Cell. Mol. Life Sci. 63 (3) (2006) 301–315.
[28] M. Sanguinetti, M. Curran, A. Zou, J. Shen, P. Specter, D. Atkinson, M. Keating, Coassembly of KvLQT1 and minK (IsK) proteins to form cardiac IKs potassium channel, Nature 384 (6604) (1996) 80–83.
[29] U. Storch, A.L. Forst, F. Pardatscher, S. Erdogmus, M. Philipp, M. Gregoritza, M.M. y Schnitzler, T. Gudermann, Dynamic NHERF interaction with TRPC4/5 proteins is required for channel gating by diacylglycerol, Proc. Natl. Acad. Sci. Unit. States. Am. 114 (1) (2017) E37–E46.
[30] S.L. Reichow, D.M. Clemens, J.A. Freites, K.L. Németh-Cahalan, M. Heyden, D.J. Tobias, J.E. Hall, T. Gonen, Allosteric mechanism of water-channel gating by Ca^{2+}-calmodulin, Nat. Struct. Mol. Biol. 20 (9) (2013) 1085–1092.
[31] X. Gong, J. Li, K. Xu, J. Wang, H. Yang, A controllable molecular sieve for Na^+ and K^+ ions, J. Am. Chem. Soc. 132 (6) (2010) 1873–1877.
[32] Z. He, J. Zhou, X. Lu, B. Corry, Bioinspired graphene nanopores with voltage-tunable ion selectivity for Na^+ and K^+, ACS Nano 7 (11) (2013) 10148–10157.
[33] W. Li, Y. Yan, M. Wang, P. Král, C. Dai, J. Zhang, Correlated rectification transport in ultranarrow charged nanocones, J. Phys. Chem. Lett. 8 (2) (2017) 435–439.
[34] W. Li, N.A. Bell, S. Hernandez-Ainsa, V.V. Thacker, A.M. Thackray, R. Bujdoso, U.F. Keyser, Single protein molecule detection by glass nanopores, ACS Nano 7 (5) (2013) 4129–4134.
[35] R. Duan, F. Xia, L. Jiang, Constructing tunable nanopores and their application in drug delivery, ACS Nano 7 (10) (2013) 8344–8349.
[36] P. Agre, Aquaporin water channels (Nobel lecture), Angew. Chem. Int. Ed. 43 (33) (2004) 4278–4290.
[37] J.D. Ho, R. Yeh, A. Sandstrom, I. Chorny, W.E. Harries, R.A. Robbins, L.J. Miercke, R.M. Stroud, Crystal structure of human aquaporin 4 at 1.8 Å and its mechanism of conductance, Proc. Natl. Acad. Sci. Unit. States Am. 106 (18) (2009) 7437–7442.
[38] S. Gravelle, L. Joly, F. Detcheverry, C. Ybert, C. Cottin-Bizonne, L. Bocquet, Optimizing water permeability through the hourglass shape of aquaporins, Proc. Natl. Acad. Sci. Unit. States Am. 110 (41) (2013) 16367–16372.
[39] S. Gravelle, L. Joly, C. Ybert, L. Bocquet, Large permeabilities of hourglass nanopores: from hydrodynamics to single file transport, J. Chem. Phys. 141 (18) (2014), 18C526.
[40] A. Barati Farimani, N. Aluru, E. Tajkhorshid, Thermodynamic insight into spontaneous hydration and rapid water permeation in aquaporins, Appl. Phys. Lett. 105 (8) (2014), 083702.
[41] L. Bocquet, P. Tabeling, Physics and technological aspects of nanofluidics, Lab Chip 14 (17) (2014) 3143–3158.
[42] A.V. Titov, B. Wang, K. Sint, P. Král, Controllable synthetic molecular channels: biomimetic ammonia switch, J. Phys. Chem. B 114 (2) (2009) 1174–1179.

[43] Y. Zhang, G.C. Schatz, Conical nanopores for efficient ion pumping and desalination, J. Phys. Chem. Lett. 8 (2017) 2842–2848.
[44] S. Plimpton, Fast parallel algorithms for short-range molecular dynamics, J. Comput. Phys. 117 (1) (1995) 1–19.
[45] W.L. Jorgensen, J. Chandrasekhar, J.D. Madura, R.W. Impey, M.L. Klein, Comparison of simple potential functions for simulating liquid water, J. Chem. Phys. 79 (2) (1983) 926–935.
[46] I.S. Joung, T.E. Cheatham III, Determination of alkali and halide monovalent ion parameters for use in explicitly solvated biomolecular simulations, J. Phys. Chem. B 112 (30) (2008) 9020–9041.
[47] T. Werder, J.H. Walther, R. Jaffe, T. Halicioglu, P. Koumoutsakos, On the water-carbon interaction for use in molecular dynamics simulations of graphite and carbon nanotubes, J. Phys. Chem. B 107 (6) (2003) 1345–1352.
[48] R.E. Smalley, B.I. Yakobson, The future of the fullerenes, Solid State Commun. 107 (11) (1998) 597–606.
[49] B. Corry, Designing carbon nanotube membranes for efficient water desalination, J. Phys. Chem. B 112 (5) (2008) 1427–1434.
[50] K. Falk, F. Sedlmeier, L. Joly, R.R. Netz, L. Bocquet, Molecular origin of fast water transport in carbon nanotube membranes: superlubricity versus curvature dependent friction, Nano Lett. 10 (10) (2010) 4067–4073.
[51] G. Hummer, J.C. Rasaiah, J.P. Noworyta, Water conduction through the hydrophobic channel of a carbon nanotube, Nature 414 (6860) (2001) 188–190.
[52] J.K. Holt, H.G. Park, Y. Wang, M. Stadermann, A.B. Artyukhin, C.P. Grigoropoulos, A. Noy, O. Bakajin, Fast mass transport through sub-2-nanometer carbon nanotubes, Science 312 (5776) (2006) 1034–1037.
[53] C.Y. Won, S. Joseph, N. Aluru, Effect of quantum partial charges on the structure and dynamics of water in single-walled carbon nanotubes, J. Chem. Phys. 125 (11) (2006), 114701.
[54] C. Dellago, M.M. Naor, G. Hummer, Proton transport through water-filled carbon nanotubes, Phys. Rev. Lett. 90 (10) (2003), 105902.
[55] M.E. Suk, N. Aluru, Water transport through ultrathin graphene, J. Phys. Chem. Lett. 1 (10) (2010) 1590–1594.
[56] C. Fang, Z. Yu, R. Qiao, Impact of surface ionization on water transport and salt leakage through graphene oxide membranes, J. Phys. Chem. C 121 (24) (2017) 13412–13420.
[57] D. Konatham, J. Yu, T.A. Ho, A. Striolo, Simulation insights for graphene-based water desalination membranes, Langmuir 29 (38) (2013) 11884–11897.
[58] Y. Chen, J. Zou, S.J. Campbell, G. Le Caer, Boron nitride nanotubes: pronounced resistance to oxidation, Appl. Phys. Lett. 84 (13) (2004) 2430–2432.
[59] E. Nightingale Jr., Phenomenological theory of ion solvation. Effective radii of hydrated ions, J. Phys. Chem. 63 (9) (1959) 1381–1387.
[60] G.M. Torrie, J.P. Valleau, Nonphysical sampling distributions in Monte Carlo free-energy estimation: umbrella sampling, J. Comput. Phys. 23 (2) (1977) 187–199.
[61] S. Kumar, J.M. Rosenberg, D. Bouzida, R.H. Swendsen, P.A. Kollman, Multidimensional free-energy calculations using the weighted histogram analysis method, J. Comput. Phys. 16 (11) (1995) 1339–1350.
[62] D. Cohen-Tanugi, J.C. Grossman, Water desalination across nanoporous graphene, Nano Lett. 12 (2012) 3602–3608.
[63] D.A. Köpfer, C. Song, T. Gruene, G.M. Sheldrick, U. Zachariae, B.L. de Groot, Ion permeation in K^+ channels occurs by direct Coulomb knock-on, Science 346 (6207) (2014) 352–355.
[64] L. Li, J. Dong, T.M. Nenoff, R. Lee, Desalination by reverse osmosis using MFI zeolite membranes, J. Membr. Sci. 243 (1) (2004) 401–404.
[65] G. Guillen, E.M. Hoek, Modeling the impacts of feed spacer geometry on reverse osmosis and nanofiltration processes, Chem. Eng. J. 149 (1) (2009) 221–231.
[66] Z. Tsakadze, I. Levchenko, K. Ostrikov, S. Xu, Plasma-assisted self-organized growth of uniform carbon nanocone arrays, Carbon 45 (10) (2007), 2022-30.
[67] V.I. Merkulov, A.V. Melechko, M.A. Guillorn, D.H. Lowndes, M.L. Simpson, Sharpening of carbon nanocone tips during plasma-enhanced chemical vapor growth, Chem. Phys. Lett. 350 (5) (2001) 381–385.